Original Article

Targeting ROS in osteoclasts within the OA environment: A novel therapeutic strategy for osteoarthritis management

Journal of Tissue Engineering
Volume 15: 1–15

DOI: 10.1177/20417314241279935
journals.sagepub.com/home/tej
Sage

Seungho Jeon[1*], Tae Min Kim[2*], Gitae Kwon[1,3*], Junyoung Park[1], Sung Young Park[2,4], Seoung Hoon Lee[3,5] and Eun-Jung Jin[1,5]

Abstract

This study investigated the therapeutic potential of a manganese dioxide-polymer dot (MnO2-PD)-incorporated hydrogel, designated as M-PD hydrogel, for modulating reactive oxygen species (ROS) within the osteoarthritis (OA) environment. Our research highlights the ability of the hydrogel to scavenge ROS, thereby influencing the differentiation of osteoclasts and protecting chondrocytes, offering a novel approach to osteoarthritis (OA) management. Our results indicated that the M-PD hydrogel increased electrical resistance and fluorescence recovery in the presence of osteoclasts, correlating with decreased ROS levels and suppressed expression of osteoclast differentiation markers. Coculture experiments revealed the protective effects of the hydrogel on chondrocytes by reducing the expression of matrix-degrading enzymes. In vivo application in burr holes and/or OA-induced mice revealed a significant reduction in osteoclast formation and cartilage destruction, suggesting the dual therapeutic action of the hydrogel in altering the joint microenvironment. These findings highlight the potential of targeting ROS in osteoclasts as a comprehensive therapeutic approach, offering not only symptomatic relief but also targeting the underlying mechanisms of disease progression in OA.

Keywords

M-PD hydrogel, osteoarthritis, osteoclast, ROS, joint microenvironment

Date received: 22 May 2024; accepted: 16 August 2024

Introduction

Osteoarthritis (OA) is a degenerative joint disease that frequently affects the elderly and is characterized by the progressive deterioration of articular cartilage and changes in trabecular bone structure.[1] This disorder often results in joint pain, stiffness, and loss of mobility, with the aging population particularly at risk due to the diminished capacity for joint repair with age. OA is a complex condition influenced by a combination of mechanical stresses, genetic factors, inflammatory processes, and cellular alterations within joint tissues. Recent findings in osteoarthritis

[1]Department of Biological Sciences, Wonkwang, University, Iksan, Jeonbuk, South Korea
[2]Department of IT and Energy Convergence (BK21 FOUR), Korea National University of Transportation, Chungju, South Korea
[3]Department of Oral Microbiology and Immunology, College of Dentistry, Wonkwang University, Iksan, Jeonbuk, Korea
[4]Department of Chemical and Biological Engineering, Korea National University of Transportation, Chungju, South Korea
[5]Integrated Omics Institute, Wonkwang University, Iksan, Jeonbuk, South Korea

*These authors contributed equally to this work.

Corresponding authors:
Sung Young Park, Department of Chemical and Biological Engineering, Korea National University of Transportation, Chungju, Chungcheongbuk-do 27469, South Korea.
Email: parkchem@ut.ac.kr

Seoung Hoon Lee, Department of Oral Microbiology and Immunology, College of Dentistry, Wonkwang University, Iksan, Jeonbuk 54538, Korea.
Email: leesh2@wku.ac.kr

Eun-Jung Jin, Department of Biological Sciences, Wonkwang, University, Rm #431, Iksan, Jeonbuk 54538, South Korea.
Email: jineunjung@wku.ac.kr

(OA) research have suggested a critical role of the dynamic interaction between osteoclasts and the cells responsible for bone resorption in trabecular bone and chondrocytes, which are the cells that form the cartilage.[2] This interaction, or osteoclast-chondrocyte crosstalk, is essential for regulating both the degradation and repair of joint tissues. Disruptions in communication and functionality can worsen OA symptoms, indicating that these interactions are foundational not only for disease progression, but also for potential treatment strategies.

Recent research has revealed that the impact of osteoclasts on cartilage extends beyond physical bone resorption to include biochemical signaling, with reactive oxygen species (ROS) emerging as crucial mediators.[3] ROS, traditionally seen as byproducts of cellular metabolism, play a pivotal role as signaling molecules. They are involved in the regulation of osteoclastogenesis and the formation of osteoclasts, which specialize in bone resorption and potentially affect chondrocyte activities, thus linking bone degradation with cartilage health in OA. The interaction between ROS and osteoclast differentiation is complex, with these molecules acting as essential secondary messengers within the cell signaling pathways that drive osteoclastogenesis.[3] Specifically, ROS produced by NADPH oxidase enzymes, such as NOX2, are known to activate key pathways including NF-κB and MAPKs. These pathways are vital for osteoclast differentiation and functionality, indicating a significant biochemical link between bone resorption and cartilage integrity in patients with OA.[4]

Reactive oxygen species (ROS) are increasingly being recognized as significant contributors to OA development.[5,6] High levels of ROS in conditions such as osteoarthritis can lead to cartilage degradation by promoting chondrocyte death, activating matrix metalloproteinases (MMPs) that break down the cartilage matrix, and inhibiting the production of key cartilage components such as collagen proteoglycans.[7] The relationship between ROS and chondrocytes is significant because chondrocytes play a crucial role in the production and renewal of the extracellular matrix.[8] In OA, the homeostatic balance of these processes is disturbed, with ROS accumulation affecting cartilage matrix catabolism.[9] Furthermore, ROS are involved in the subchondral bone alterations observed in OA by affecting osteoclasts.[10] These cells are essential for bone remodeling, a dynamic process of bone formation and resorption that maintains bone health.[11] Osteoclast activity is often upregulated,[12] resulting in abnormalities in the trabecular bone, which contribute to joint pain and dysfunction.[12] Given the harmful effects of ROS in OA, strategies to reduce ROS levels have emerged as a compelling therapeutic approach. Several studies have explored the use of bisphosphonates, which are potent inhibitors of osteoclast-mediated bone resorption.[13,14] These agents have demonstrated efficacy in reducing bone turnover, alleviating pain, and preserving joint structure in preclinical OA models and clinical trials. Additionally, denosumab, a monoclonal antibody that targets RANKL (receptor activator of nuclear factor kappa-B ligand), has been investigated for its potential to improve joint integrity in OA patients. Another therapeutic approach involves the use of cathepsin K inhibitors, which block the activity of a protease critical for osteoclast function. These inhibitors have been found to reduce bone resorption and cartilage damage in animal models of OA. Moreover, neutralization of ROS, known as ROS scavenging, can be achieved using various methods, including natural antioxidants, enzymatic antioxidants, and synthetic scavengers.[15] Among these, biomaterial-based delivery systems offer a promising approach owing to their biocompatibility, ability to encapsulate and release therapeutic agents or cells,[16,17] and ability to specifically target areas within the joint.[18,19] The primary objective of this study was to evaluate the efficacy of M-PD hydrogel in scavenging reactive oxygen species (ROS), thereby altering the cellular microenvironment to suppress osteoclast differentiation and enhance chondrocyte viability. Manganese dioxide (MnO2) nanoparticles are well-known for their high catalytic activity in decomposing ROS. The incorporation of MnO2 into the hydrogel matrix enhances the material's ability to neutralize ROS, which are elevated in the osteoarthritic joint environment and contribute to inflammation and tissue degradation. This dual-modality approach aimed to determine the pathological balance required to preserve joint integrity and function. Our study demonstrated that when the ROS-scavenging hydrogel was implanted in the tibia, it could simultaneously regulate chondrocyte function and osteoclast differentiation, thus exerting a protective effect against the onset and progression of osteoarthritis (OA; Figure 1). Additionally, the hydrogel matrix provides a biocompatible and stable environment for the MnO2 nanoparticles, ensuring sustained ROS scavenging activity over time. This stability is crucial for chronic conditions like OA, where long-term treatment is necessary. Moreover, the hydrogel can be locally applied to the affected joint, allowing for targeted delivery of the therapeutic agents. This localized treatment minimizes potential side effects and maximizes the therapeutic impact on the joint tissues.

Materials and methods

Materials

Hyaluronic acid (HA, $M_w = 100{,}000$ Da), polyvinyl alcohol (PVA, $M_w = 125{,}000$ Da), poly(vinyl pyrrolidone; PVP, $M_w = 55{,}000$), potassium permanganate ($KMnO_4$), 2-chloro-3,4-dihydroxyacetophenone (CCDP), 1,3-propanesultone 98%, anhydrous ethanol, *n*-hexane, anhydrous tetrahydrofuran, and diethyl ether were purchased from Sigma–Aldrich. Polymer dots were synthesized by hydrothermal carbonization of PVP-CCDP. An MnO_2-PD-incorporated

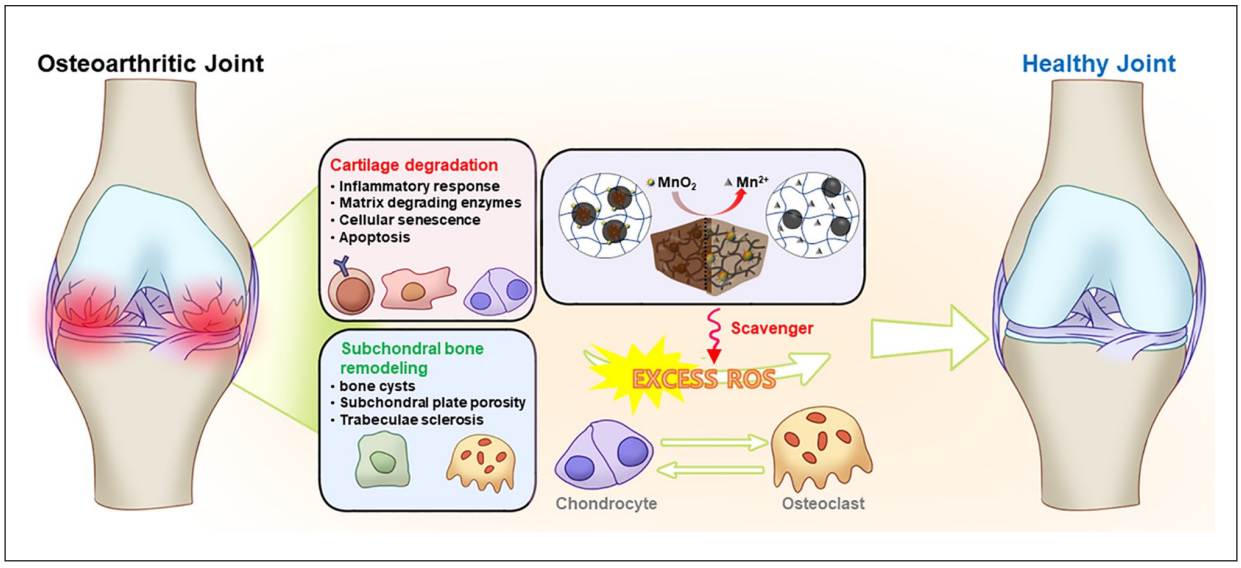

Figure 1. Graphical abstract of the study.

ROS-responsive hydrogel (M-PD hydrogel) was fabricated using a previously reported method.[20] Soluble recombinant mouse RANKL and recombinant human M-CSF used in osteoclastogenesis in this study were a gift from Dr. T Kim (KIOM, Daejeon, Korea).

Conductivity response of M-PD hydrogel

The conductivity changes of the M-PD hydrogel before and after treatment with osteoclast chondrocytes were measured using an electrochemical impedance spectrometer (EIS; CS350, CorrTest Instrument, China) with a two-electrode system in the frequency range of 10^4–10^{-1} Hz and a measurement polarity of 0 V versus the open circuit potential (OCP). The resistance of the M-PD hydrogels was measured using a 2-electrode DC system source meter (Keithley 2450, Tektronik, USA).

Confocal imaging of M-PD hydrogel

After in vitro and in vivo experiments, the fluorescence properties of the M-PD hydrogel were observed using a confocal microscope (ECLIPSE Ti2-E, Nikon, Tokyo, Japan). To prepare the samples for measurement, the hydrogel was sliced to a thickness of 1 mm. The hydrogel was then placed under the confocal microscope and the fluorescence were determined using a $\lambda = 405$ mm laser.

iMAC isolation and culture

Primary articular chondrocytes were extracted from mice aged 5 to 6 days by dissecting the femoral condyles and tibial plateaus. The isolated cartilage undergoes an initial 45-min digestion in a solution of 3 mg/mL collagenase D (Roche), followed by overnight digestion in 0.5 mg/mL collagenase D at 37°C. After digestion, the suspension was filtered through a 70-μm cell strainer to separate the primary chondrocytes. These cells were cultured in Dulbecco's modified Eagle's medium (DMEM; Gibco-Invitrogen) supplemented with 10% fetal bovine serum (FBS; Gibco-Invitrogen) and antibiotics (100 units/mL penicillin and 100 units/mL streptomycin).

In vitro osteoclastogenesis

Osteoclasts were formed from bone marrow cells (BMs) using stromal cell-free cultures. Briefly, BMs were extracted from the femurs and tibias of C57BL/6N mice and cultured in MEM-α with 10% FBS and M-CSF (30 ng/mL) for 3 days, yielding bone marrow-derived macrophages (BMMs) for use as osteoclast precursors. For osteoclast generation without stromal cells, BMMs were cultured for 4 days in MEM-II supplemented with 10% FBS, M-CSF (30 ng/mL), and RANKL (100 ng/mL), and media changes with RANKL and M-CSF were performed on day 3. The cells were then fixed with 10% formalin and permeabilized with 0.1% Triton X-100 in phosphate-buffered saline (PBS) for assay of TRAP activity. After TRAP solution assay, the cell was washed with PBS and stained for TRAP with Naphthol-AS-BI-phosphate and Fast red violet LB (Sigma-Aldrich, St. Louis, MO, USA). Mature osteoclasts were identified as TRAP(+) multinuclear cells (MNCs) having actin ring and larger than 100 μm with over three nuclei.

Measurement of ROS levels

Bone marrow cells were cultured for 3 days under M-CSF treatment to produce bone marrow-derived macrophages (BMMs). These BMMs were further cultured with M-CSF for 1 day to maintain osteoclast precursor status, or with

M-CSF and RANKL for 4 days to develop mature osteoclasts. Subsequently, the cells were preincubated with either a control solution or M-PD hydrogel for 2 h. Following preincubation, the cells were washed with HBSS (Hank's Balanced Salt Solution) and incubated in the dark for 10 min in HBSS containing 10 μM DCF-DA (2′,7′-dichlorofluorescin diacetate). The culture plates were then transferred to a fluorescence inverted microscope (Leica DM IL LED, Wetzlar, Germany) for fluorescence imaging. The relative fluorescence intensity of the images from each group was analyzed using ImageJ software (version 1.53, NIH, USA).

Radical scavenging assay

DPPH assay, •OH scavenging assay, scavenging, and $O2^{\bullet-}$ scavenging assay were performed to confirm the antioxidant property of the hydrogel. For the DPPH assay, 3 mL of DPPH solution (0.1 mM) and hydrogel were incubated at 37°C for 45 min. Superoxide radical scavenging activity was measured by mixing 2 mL of xanthine (0.6 mM) and 1 mL of xanthine oxidase (0.05 U/mL) at 37°C for 10 min, then adding hydrogel and mixing for 30 min. Then, another 2 mL of iodonitrotetrazolium chloride (0.05 mg/mL) was added. For the hydroxyl radical scavenging assay, the hydrogel was mixed with 1 mL of salicylic acid (6 mM), PBS (pH 7.4), FeSO4 (6 mM, 1 mL), and H_2O_2 (0.01%, 0.5 mL) and incubated at 37°C for 30 min. Each scavenging activity was calculated by measuring the absorbance of the incubated assay solution using UV-Vis spectroscopy at the wavelengths of 517 nm (DPPH assay), 505 nm (•OH scavenging assay), and 510 nm (O2•− scavenging assay).

Cell viability assay

Cell viability was assessed using the EZ-Cytox Enhanced Cell Viability Assay Kit (Itsbio, Korea) according to the manufacturer's instructions. Bone marrow-derived macrophages (BMMs) were cultured in the presence of M-CSF (30 ng/mL) at a density of 1×10^5 cells/well in 24-well plates and C2C12 cells and human dermal fibroblasts (HDFs) were cultured at a density of 7×10^4 cells/well in 24-well plates were cultured with either control gel or M-PD hydrogel for 12 h. At the assay endpoint, the cells were incubated with EZ-Cytox reagent for 4 hrs at 37°C. Following incubation, cell viability was quantified by measuring the optical density at 450 nm using an ELISA reader (Sunrise™, Tecan). The viability of the cells was expressed as a relative percentage compared to the vehicle-treated control group (no gel).

Western blot analysis

The total lysates (30 μg) were separated by SDS-PAGE and transferred to PVDF membranes (Amersham Hybond-P) or Nitrocellulose membrane (Amersham). The membranes were blocked with 5% skim milk in TBST (50 mM Tris-HCl, pH = 7.6, 150 mM NaCl, and 0.1% Tween-20) and incubated with primary antibodies against NFATc1 (Santa Cruz Biotechnology) or MMP-9 (Abcam) at a 1:1000 dilution. HRP-conjugated secondary antibodies (1:5000 dilution) were used for detection. Immunoreactive proteins were visualized using an ECL detection system (Thermo Fisher Scientific) according to the manufacturer's instructions. Band intensities were quantified using ImageJ 1.53 software and expressed as relative fold changes.

Gelatin zymography

Cells were incubated in serum free medium for 24 h and Total protein content (Pierce Biotechnology) and cell number was determined. Loading amounts were standardized to either the lowest protein concentration or cell number for all samples from that particular iteration of the experiment. Then, the CM was concentrated by 10% (v/v) trichloroacetic acid precipitation. The precipitate was dissolved in 1× nonreducing sample buffer (62.5 mM Tris/HCl, pH 6.8, containing 10% glycerol, 2% (w/v) SDS and 0.005% Bromophenol Blue) and subjected to SDS/7.5% PAGE co-polymerized with gelatin (0.1%) as the substrate. After electrophoresis, the gel was incubated for 10 min at room temperature in a 2.5% Triton X-100 solution and incubated at 37◦C for overnight in 50 mM Tris-HCl buffer (pH 7.5) containing 5 mM $CaCl_2$, 1 μM $ZnCl_2$. The gels were stained with 0.05% Coomassie Brilliant Blue R-250, 50% ethanol and 10% acetic acid and then destained with 25% ethanol and 10% acetic acid. Gelatinolytic activities were detected as unstained bands against the background of Coomassie Blue-stained gelatin.

Real-time polymerase chain reaction

Total RNA was extracted from each cultured cell at specified time points using Trizol reagent (Thermo Fisher Scientific). Cells were lysed directly in the culture dish by adding 1 mL of Trizol reagent per 10 cm^2 of culture dish surface area and homogenized by pipetting up and down. The lysates were incubated for 5 min at room temperature, followed by the addition of 0.2 mL of chloroform per 1 mL of Trizol reagent. The mixture was shaken vigorously for 15 s, incubated for 3 min at room temperature, and centrifuged at 12,000*g* for 15 min at 4°C. The aqueous phase containing RNA was transferred to a new tube, mixed with 0.5 mL of isopropanol per 1 mL of Trizol reagent, incubated for 10 min at room temperature, and centrifuged at 12,000*g* for 10 min at 4°C. The RNA pellet was washed with 1 mL of 75% ethanol per 1 mL of Trizol reagent, vortexed briefly, and centrifuged at 7500*g* for 5 min at 4°C. The RNA pellet was air-dried for 5-10 min and dissolved in RNase-free water, and its concentration and purity were

determined using a Nanodrop spectrophotometer. For cDNA synthesis, 1 μg of total RNA was transcribed into first strand cDNA using the Maxima First Strand cDNA Synthesis Kit (Thermo Fisher Scientific) according to the manufacturer's instructions. The reaction mixture included 4 μL of 5× reaction mix, 2 μL of Maxima enzyme mix, and RNase-free water to a final volume of 20 μL. The mixture was incubated at 25°C for 10 min, 50°C for 30 min, and 85°C for 5 min.

Real-time PCR assays were performed using the VeriQuest SYBR Green qPCR Master Mix (Affymetrix, Santa Clara, CA, USA). Each reaction contained 10 μL of VeriQuest SYBR Green qPCR Master Mix, 0.5 μL of forward primer (10 μM), 0.5 μL of reverse primer (10 μM), 2 μL of cDNA template, and 7 μL of RNase-free water, making a total volume of 20 μL. PCR was carried out on a StepOnePlus Real-Time PCR System (Applied Biosystems) with the following cycling conditions: initial denaturation at 95°C for 10 min, followed by 40 cycles of denaturation at 95°C for 15 s, and annealing/extension at 60°C for 1 min. Data were normalized using glyceraldehyde 3-phosphate dehydrogenase (*Gapdh*) or 18S rRNA. The primers used in this study are listed in Supplementary Table 1.

Animals

Wild-type C57BL/6N mice were purchased from Samtako BioKorea, Inc. (Osan, Korea). Upon arrival, the mice were acclimated for 1 week in the animal facility to reduce transport-related stress. All mice were housed in a controlled environment maintained at 23 ± 1°C with a 12-h light/dark cycle and a relative humidity of 50 ± 5%. Standard rodent chow and water were provided ad libitum. Mice were housed in groups of three to four per cage, with nesting material and environmental enrichment provided to promote natural behaviors and reduce stress. The health and well-being of the animals were monitored daily, and any signs of distress or illness were promptly addressed by veterinary staff. All experimental procedures involving animals were conducted in accordance with the guidelines and regulations approved by the Institutional Animal Care and Use Committee (IACUC) of Wonkwang University (#WKU23-21), ensuring ethical treatment and care throughout the study.

Burr-hole for bone defect

To create a burr-hole bone defect, we adapted previously reported protocols with minor modifications.[21] Mice were anesthetized using an appropriate anesthesia protocol (e.g. isoflurane inhalation) to ensure they were fully unconscious and immobile during the procedure. The surgical site was shaved and sterilized using betadine and 70% ethanol to minimize the risk of infection.

A small incision was made on the lateral (medial) side of the right knee using a sterile scalpel. A high-speed microdrill (Harvard Apparatus, Holliston, MA, US) equipped with a 0.8 mm burr was used to create the defect. The drill was carefully positioned perpendicular to the lateral cortex of the tibia and operated at a moderate speed to penetrate the cortical bone without generating excessive heat, which could damage surrounding tissues. The drilling process was stopped as soon as the burr penetrated the cortical bone and reached the medullary cavity of the lateral metaphyseal trabecular region. After creating the hole, the drill was withdrawn carefully, and the area was inspected to ensure that the defect was properly formed. The surgical site was rinsed with sterile saline to remove any bone debris and ensure a clean working area. Depending on the experimental group, the M-PD hydrogel or control gel was applied directly into the burr hole. A small amount of gel was carefully placed to ensure it filled the defect without overflowing. The mice were allowed to recover from anesthesia under a heat lamp to maintain body temperature. Postoperative care included monitoring for signs of infection or distress and providing analgesics as needed to ensure the animals' well-being.

Experimental OA and histology of OA cartilage

Osteoarthritis (OA) was experimentally induced in mice by destabilizing the medial meniscus (DMM). Following the induction of OA, knee joints were harvested and fixed in 4% paraformaldehyde to preserve tissue architecture. The fixed tissues were then decalcified using 14% EDTA at pH 7.4 to remove mineral content and allow for proper sectioning. After decalcification, the samples underwent a dehydration process through a graded series of ethanol, cleared with xylene, and then infiltrated with paraffin to enable embedding. The tissues were subsequently embedded in paraffin blocks. Paraffin blocks were sectioned into 5-μm thick slices, which were mounted onto microscope slides. These sections were stained with safranin O to visualize and assess cartilage integrity, as safranin O stains the glycosaminoglycans in cartilage matrix. The extent of cartilage degradation in the stained sections was evaluated using the Osteoarthritis Research Society International (OARSI) scoring system. This system scores cartilage damage on a scale from 0 to 6, where 0 represents no damage and 6 indicates severe damage. This scoring method allowed for a standardized and quantitative assessment of cartilage degradation in the OA model.

Histological staining of bone

To assess the effect of the M-PD hydrogel in in vivo bone and cartilage defect models, excised bones from the burr-hole and burr-hole/DMM groups were fixed in 4% paraformaldehyde for 2 days. After fixation, the bones were decalcified in 12% EDTA until they became pliable and

then embedded in paraffin. Subsequently, 5 μm thick sections were prepared. TRAP staining was performed on these sections to visualize osteoclasts, following a previously established protocol. For TRAP staining, the sections were deparaffinized and rehydrated through a graded series of ethanol. The sections were then incubated in a TRAP staining solution, prepared according to the manufacturer's instructions, to specifically stain for osteoclasts. Following staining, the sections were counterstained with hematoxylin to visualize the nuclei. Histological analysis of TRAP-stained sections involved counting the number of TRAP-positive multinucleated osteoclasts per section. Photographs of the stained bones were captured using a Leica light microscope (Leica, Wetzlar, Germany). Quantitative analysis of the osteoclasts was conducted using ImageJ software (Version 1.53, NIH, USA).

Immunohistochemistry

For immunohistochemistry, deparaffinized and rehydrated paraffin sections underwent antigen retrieval was performed with deparaffinized rehydrated paraffin sections using 0.01 M sodium citrate buffer (0.05% Tween 20, pH 6.0). Non-specific antibody-binding sites were blocked by incubation with 2.5% normal horse serum from the ImmPRESS Universal Antibody Kit (Vector Laboratories). The sections were incubated overnight with antibodies against MMP13 (1:200 dilution, BioVision; #3533), F4/80 (1:200 dilution, Thermo Scientific, MA5-16624), caspase 3 (1:200 dilution, Cell Signaling, #9662P), or Ki67 (1:200 dilution, Abcam, Ab16667). After incubation with a peroxidase-conjugated secondary antibody for 30 min, the antigen was detected using the ImmPACT DAB Substrate (Vector Laboratories).

Results

Modulating osteoclast differentiation and ROS levels: A novel MnO2-PD hydrogel approach

In this study, we explored the effects of an ROS-scavenging hydrogel embedded with Manganese Dioxide-Polymer Dot (MnO_2-PD or M-PD) nanoparticles on osteoclast differentiation. In our previous work,[22] we characterized the properties of a hydrogel containing Dioxide-Polymer Dot (MnO_2-PD or M-PD) nanoparticles, specifically examining viscoelastic strain sweep and tensile mechanics both before and after treatment with H_2O_2. Additionally, SEM images highlighted the impact of H_2O_2 on the microstructure of the hydrogel. In this study, further analysis was conducted as described in Supplementary Figure 1 where TEM images of the M-PD hydrogel showed a reduction in the particle size of MnO_2-PD due to H_2O_2 exposure. This change in morphology confirms the cleavage and disintegration of MnO_2 with PD. We also performed a degradation rate analysis to evaluate the stability of the M-PD hydrogel. As shown in Supplementary Figure 2, the hydrogel displayed a degradation rate of $0.19 \pm 0.01\%$ over 2 days in a 0 mM H_2O_2 environment, indicating high stability suitable for animal experiments. In contrast, in a 0.1 mM H2O2 environment, the degradation rate increased to $1.59 \pm 0.17\%$ over the same period, suggesting a slight acceleration in degradation as MnO2 decomposed to Mn2+. Moreover, we analyzed the mechanical properties of the M-PD hydrogel post-H_2O_2 treatment. The compressive strength of the hydrogel decreased after exposure to H_2O_2 (see Supplementary Figure 3(a)), while the elasticity increased due to the reduction of MnO_2 to Mn2+. Additionally, a frequency sweep test was conducted to determine the viscoelastic behavior of the hydrogel (see Supplementary Figure 3(b)). The storage modulus (G') was found to be higher than the loss modulus (G''), across the assumed frequency range, confirming a significant shift in the elastic properties of the hydrogel post-H_2O_2 treatment. These findings provide a deeper understanding of the physicochemical properties of M-PD hydrogels under oxidative conditions. The antioxidant effect of MnO2 in the M-PD hydrogel was confirmed by a radical scavenging assay (Supplementary Figure 4). The DPPH inhibition effect (77.8%), superoxide radical scavenging activity (93.1%), and hydroxyl radical scavenging activity (84.4%) of the M-PD hydrogel demonstrated excellent antioxidant properties compared to the control hydrogel. We induced bone marrow-derived macrophages (BMMs) to transform into osteoclasts using macrophage colony-stimulating factor (M-CSF) and receptor activator of nuclear factor kappa-B ligand (RANKL) in the presence of M-PD hydrogel (Figure 2(a)). We assessed the electrical resistance of the M-PD hydrogel over time during cell culture using a sourcemeter and electrochemical impedance spectroscopy (EIS), measuring resistance with incubation intervals (D1→D2, D2→D3, D3→D4) to observe the effects of osteoclast differentiation on the hydrogel's conductivity. A control hydrogel lacking M-PD nanoparticles used as the comparison group, showing no significant resistance change over time, with values at 41.4 kΩ (D1 → D2), 41.0 kΩ (D2 → D3), and 41.6 kΩ (D3 → D4). Conversely, the M-PD hydrogel exhibited an increase in resistance, indicating resistance values of 23.9 kΩ (D1 → D2), 25.1 kΩ (D2 → D3), and 26.4 kΩ (D3 → D4).

Nyquist plots from the EIS analysis revealed that the resistance changes in the control gel were minimal, whereas the M-PD hydrogel showed a progressive increase in resistance, correlating with incubation duration. Moreover, the LED experiment demonstrated a decrease in the light intensity of the LED lamp connected to the M-PD hydrogel as the resistance increased, unlike the LED connected to the control gel, which maintained an unchanged light intensity (Figure 2(b)). Confocal imaging revealed that the optical properties of the M-PD hydrogel

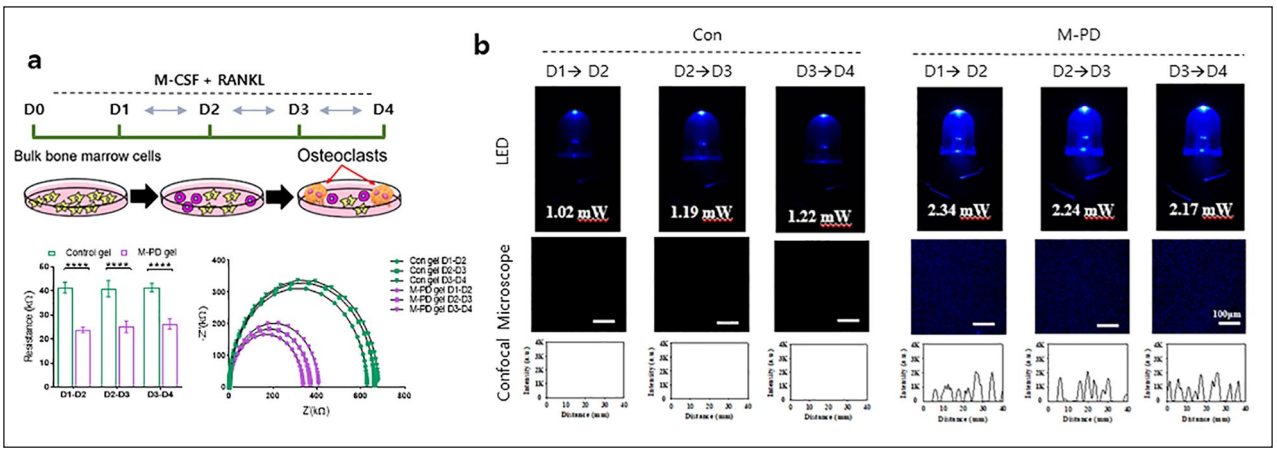

Figure 2. Effects of ROS scavenging hydrogel on osteoclast differentiation. BMMs were differentiated into osteoclasts with 30 ng/mL M-CSF and 100 ng/mL RANKL treatment in the presence of Control gel (Con) and M-PD hydrogel for indicated time (culture days 1–3 (D1 → D2), culture days 2–3 (D2 → D3), and culture days 3–4 (D3 → D4)), $n = 3$ per group. (a) Electrical resistance measurement by sourcemeter and electrochemical impedance spectroscopy (EIS). (b) LED intensity and confocal microscopy analysis.

changed with increased fluorescence recovery, a phenomenon that was not observed in the control gel (Figure 2(b)). These shifts in the electrical and optical characteristics of the hydrogel are attributed to elevated ROS levels as osteoclast development progresses, resulting in increased MnO2 breakdown. This decreases the conductivity of the hydrogel and releases PD, thereby inducing fluorescence recovery. ROS staining of BMMs further demonstrated that treatment with the M-PD hydrogel lowered the cellular ROS levels, indicating its scavenging capability (Figure 3(a)). Additionally, osteoclast differentiation was notably inhibited in the presence of M-PD hydrogel, as shown by diminished Tartrate-resistant acid phosphatase (TRAP) activity and the number of TRAP(+)-multinuclear mature osteoclasts (Figure 3(b)). Additionally, the expression level of crucial markers and transcription factors for osteoclast differentiation, including *TRAP, Cathepsin K (CTSK), Osteoclast Associated Ig-like Receptor (OSCAR), V-ATPase V0 domain subunit d2 (Atp6v0d2), Dendritic cell-specific transmembrane protein (DC-STAMP)*, and *nuclear factor of activated T cells 1 (NFATc1)* was dramatically downregulated by M-PD hydrogel treatment (Figure 4). The hydrogel also affected cellular oxidative defenses by decreasing the expression of *Superoxide Dismutase (SOD)1* and *SOD2*, indicating its role in the regulation of both external and internal ROS levels.

Combating osteoarthritis with ROS-responsive hydrogels: Insights into osteoclast-chondrocyte interplay

Given that reduced osteoclast function can prevent the breakdown of articular cartilage, thereby slowing osteoarthritis (OA) progression, we hypothesized that a ROS-scavenging hydrogel could play a crucial role in a comprehensive treatment strategy aimed at preserving joint integrity and function in patients with OA. To test this hypothesis, we explored the effect of the M-PD hydrogel on the intricate interplay between osteoclasts and chondrocytes.

To explore the role of osteoclasts in OA development, we conducted co-culture experiments with RANKL-induced osteoclasts and chondrocytes. First, BMMs were cultured with M-CSF and RANKL for 3 days to induce the formation of mature osteoclasts. They were then incubated with M-PD hydrogel and co-cultured with osteoarthritis (OA) chondrocytes in a transwell culture plate. The in vitro OA model was established by adding IL-1β to the chondrocytes. Control gel (Con-gel) lacking M-PD nanoparticles showed no significant resistance changes under both normal and OA conditions (Normal-Con gel: 40.5 kΩ, OA-Con gel: 40.2 kΩ). However, the resistance of the M-PD hydrogel in OA conditions (OA-M-PD hydrogel: 29.6 kΩ) decreased significantly after MnO2 converted to Mn2+ in the presence of osteoclasts (Figure 5(a)). The change in fluorescence properties of the M-PD hydrogel under OA conditions was further confirmed through confocal images, in which the Con-gel possessed no fluorescence under both normal and OA conditions, whereas the M-PD hydrogel exhibited fluorescence recovery under OA conditions (Figure 5(b)), confirming its capability to detect osteoclast occurrence in the OA model through MnO2-ROS interaction.

The co-culture of OA chondrocytes and osteoclasts in the M-PD hydrogel significantly suppressed osteoclastogenesis (Figure 5(c)). The treatment led to a marked reduction in the number of mature osteoclasts and TRAP activity, along with decreased expression levels of ROS-related genes *SOD1* and *SOD2* and osteoclast differentiation markers, *TRAP,*

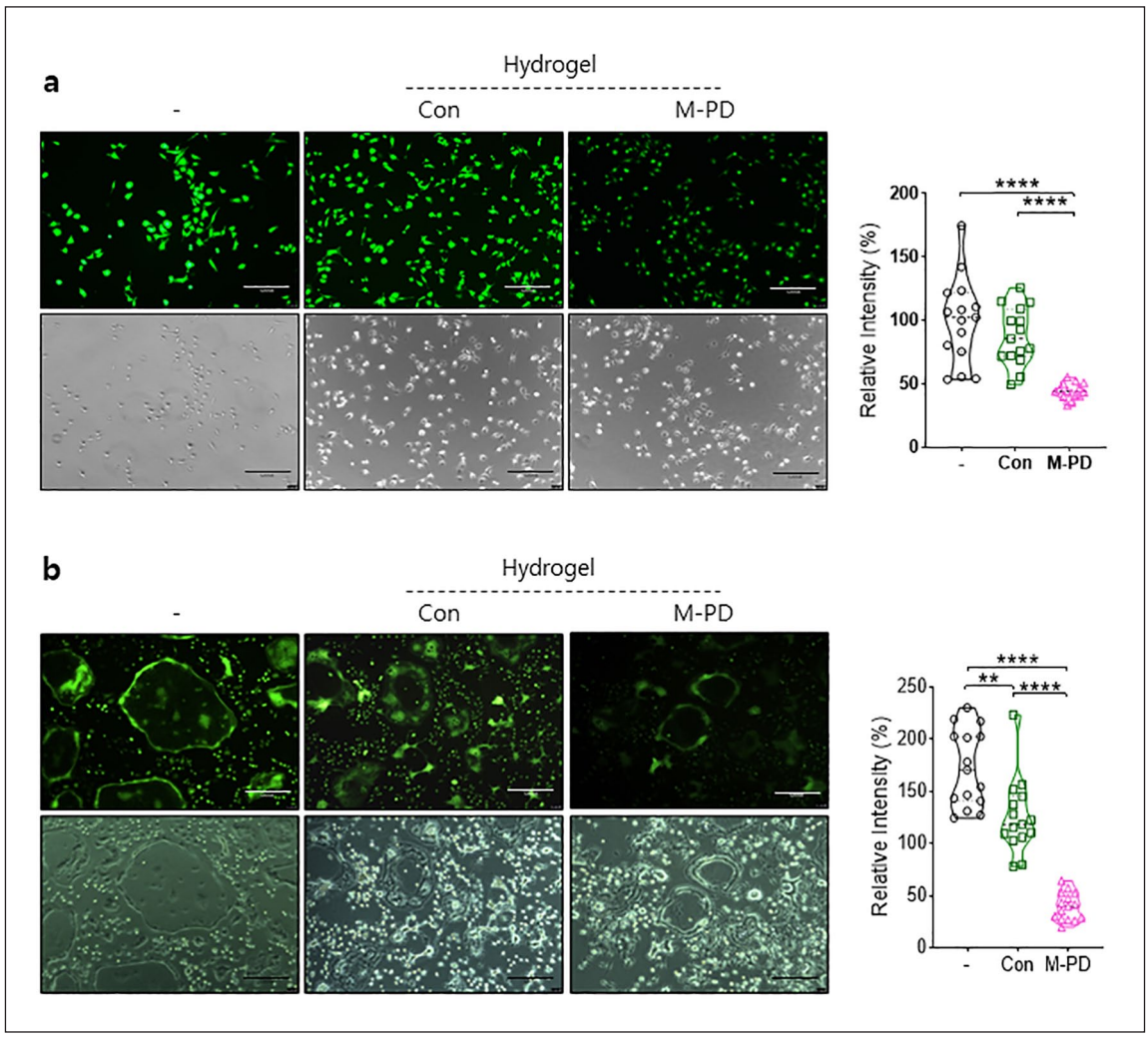

Figure 3. The effect of M-PD hydrogel on RANKL-induced ROS production in BMMs and osteoclasts. (a) ROS production assay using by DCF-DA treatment on BMMs under M-CSF induction for 1 day, followed by incubated with Control and M-PD hydrogel for 2 hr. (b) ROS production assay on Osteoclasts cultured for 3 days under M-CSF and RANKL treatment, followed by Control and M-PD hydrogel addition for 2 h. Mean ± SEM, $^{**}p < 0.01$, and $^{****}p < 0.0001$, N.S, not significant by Student's *t* test.

DC-STAMP, and *NFATc1* (Figure 5(d)). There was a notable decrease in the expression of enzymes responsible for cartilage matrix degradation, such as *Matrix metalloproteinase-9* (*MMP-9*), *A disintegrin and metalloproteinase with thrombospondin motifs* (*ADAMTS*)*4*, and *ADAMTS5* in OA chondrocytes co-cultured with osteoclasts in the M-PD hydrogel. Furthermore, protein level of NFATc1 in osteoclast as well as the expression and activation level of MMP-9 in OA chondrocyte, were also significantly decreased with the application of M-PD hydrogel (Figure 5(e)). This reduction suggests that ROS scavenging not only affects osteoclasts, but also protects cartilage by diminishing the expression of degradative enzymes.

To further validate the role of ROS in regulating the interactions between osteoclasts and osteoarthritic chondrocytes, we applied *N*-acetyl-L-cysteine (NAC), a known ROS-scavenging activator. BMMs were cultured with M-CSF and RANKL in presence of NAC for 4 days. Consistent with previous reports,[23] NAC treatment significantly inhibited osteoclast differentiation (Figure 6(a)). There was also an increase in Alcian Blue staining in chondrocyte cultures, indicating enhanced cartilage matrix production and a significant reduction in the expression of the cartilage matrix-degrading enzyme MMP-3 (Figure 6(b)). However, in chondrocytes, the administration of NAC did not alter the expression levels of *SOD1* and *SOD2*. Administration of NAC in co-culture experiments also resulted in increased *SOD* expression in osteoclasts, suggesting a decrease in intracellular ROS levels and, consequently, reduced osteoclast differentiation and chondrocyte degeneration (Figure 6(c)). These findings underscore the potential of modulating ROS levels as a novel approach for managing OA progression, offering the dual therapeutic benefit of protecting cartilage while inhibiting bone degradation by targeting ROS in osteoclasts with a scavenging gel.

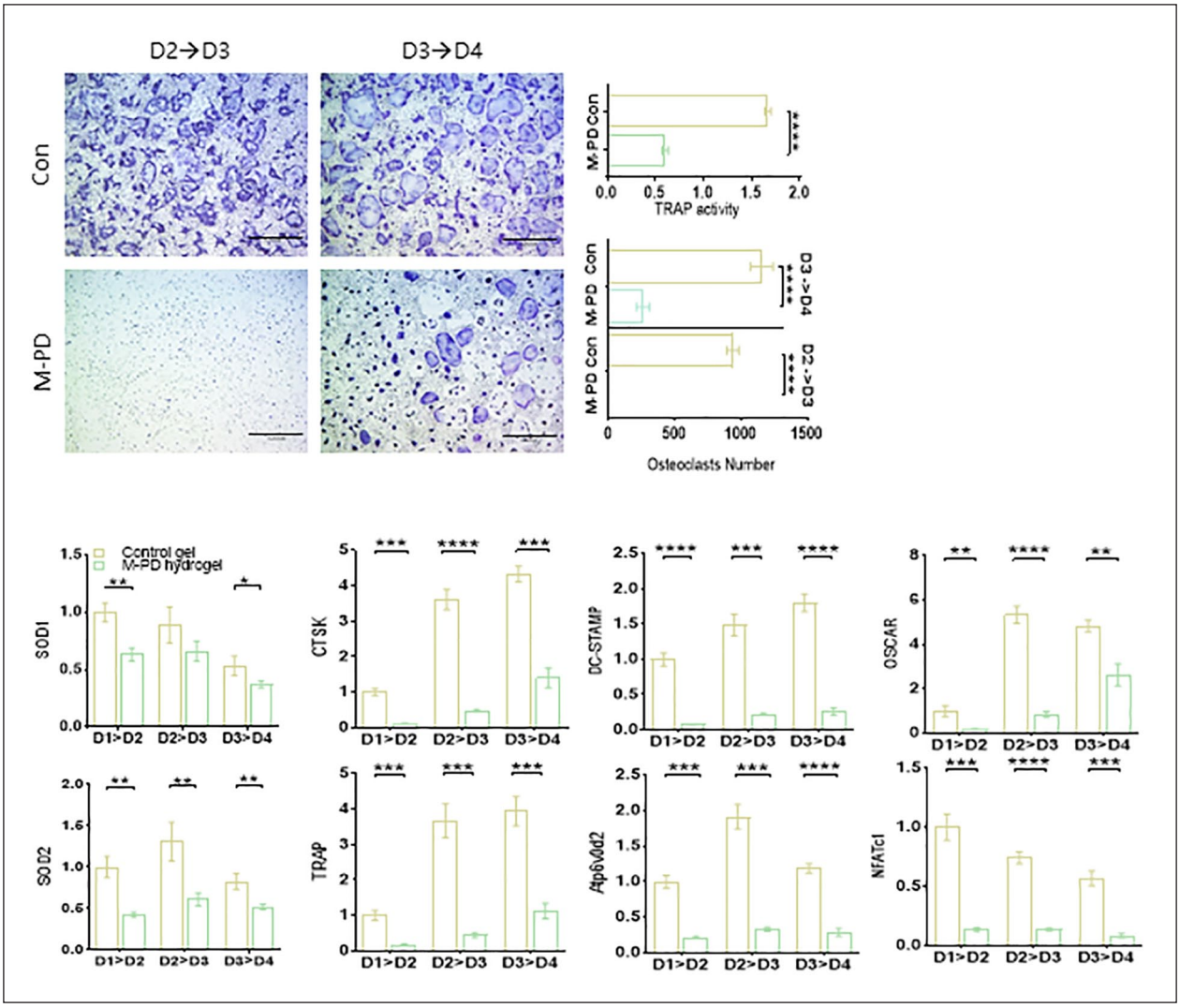

Figure 4. Effects of ROS scavenging hydrogel on osteoclast differentiation. BMMs were differentiated into osteoclasts with 30 ng/mL M-CSF and 100 ng/mL RANKL treatment in the presence of Control gel (Con) and M-PD hydrogel for indicated time (culture days 1–3 (D1 → D2), culture days 2–3 (D2 → D3), and culture days 3–4 (D3 → D4)), $n = 3$ per group. Representative TRAP staining images of osteoclasts in the presence of Con or M-PD gel for D2 → D3, and D3 → D4. Quantification of TRAP activity, the number of TRAP+-multinuclear cells. The expression level of anti-oxidant gene (*SOD1* and *SOD2*) osteoclast differentiation markers (*TRAP, CTSK, OSCAR, ATP6v0d2*, and *DC-STAMP*) and transcription factors (*NFATc1*) was measured by RT-PCR. Values are Mean ± SD, $^{*}p < 0.05$, $^{**}p < 0.01$, $^{***}p < 0.001$, $^{****}p < 0.0001$, N.S, not significant by Student's *t* test.

Innovating osteoarthritis treatment: Insights into the dual therapeutic action of ROS-scavenging M-PD hydrogel redefining osteoarthritis management

An in vivo model was used to assess the effectiveness of the M-PD hydrogel in modulating osteoclasts and mitigating the cartilage matrix deterioration. A burr hole was created in the tibia of normal or osteoarthritis (OA)-induced mice onto which the hydrogel was applied (Figure 7). OA was induced in mice by the destabilization of Medial Meniscus (DMM) surgery. The in vivo electrochemical sensing capabilities of the M-PD hydrogel were evaluated by implanting it into OA mice, which were divided into two groups (Burr Hole and DMM/Burr Hole) and comparing the outcomes with a control gel (Figure 7(a)). The Control gel showed negligible changes in resistance across all groups (Burr Hole_Con gel: 56.6 kΩ, DMM/Burr Hole_Con gel: 54.1 kΩ). Conversely, the M-PD hydrogel groups exhibited a significant increase in resistance compared to pre-implantation levels (15.0 kΩ), with readings of 33.3 kΩ (Burr Hole_M-PD hydrogel), and 42.1 kΩ (DMM/Burr Hole_M-PD hydrogel). This increase in resistance, especially in the OA mice treated with the DMM/Burr Hole_M-PD hydrogel, was attributed to the high ROS levels cleaving MnO2, thus reducing conductivity. This decrease in conductivity was visually confirmed using an LED lamp connected to the implanted M-PD hydrogel,

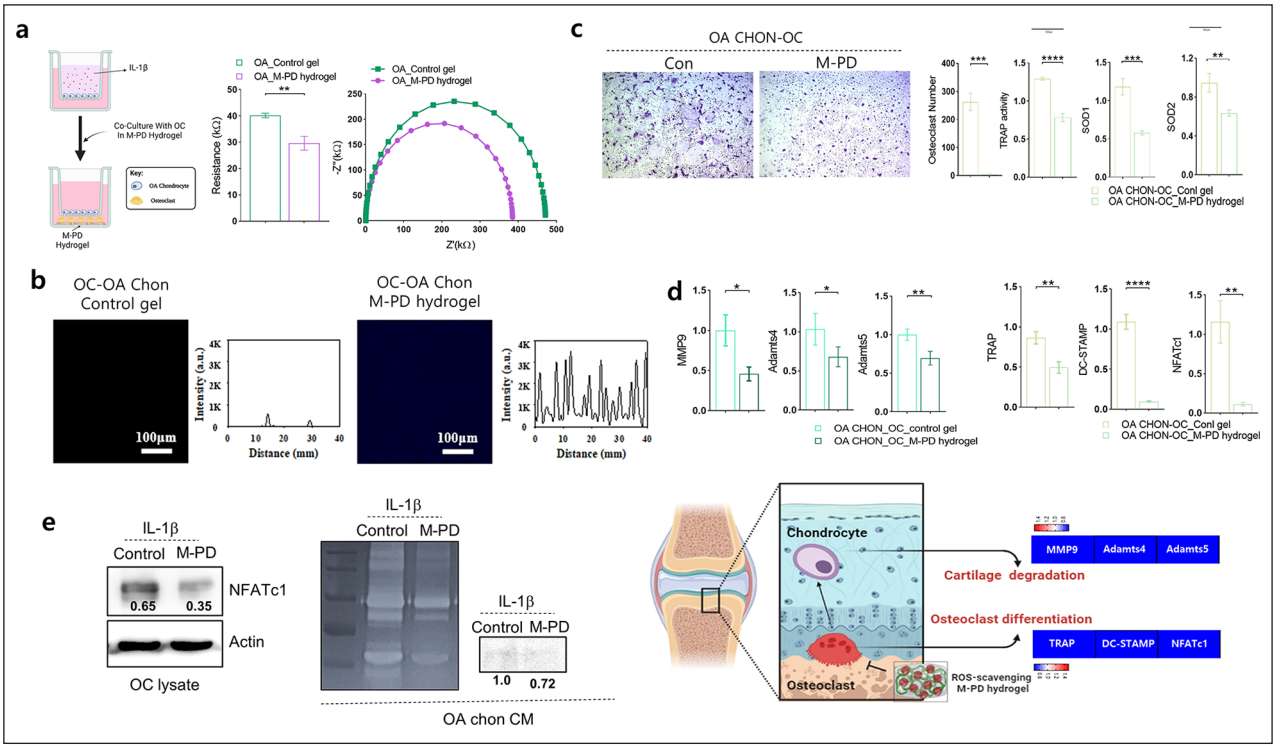

Figure 5. Modulation of osteoclasts and chondrocytes interactions via ROS scavenging hydrogel. BMMs were incubated with M-CSF and RANKL for 3 days to form mature osteoclasts, then osteoclasts were co-cultured with OA chondrocytes in presence of control (Con) or M-PD hydrogel. $n = 3$ per group. (a) The schematic diagram of the experimental setup for osteoarthritis (OA) chondrocyte-osteoclast co-culture with the M-PD hydrogel and Electrical resistance and impedance spectroscopy. (b) Fluorescence microscopy analysis. (c) Representative TRAP staining images of osteoclasts in Con or M-PD gel co-cultured with OA-chondrocytes. TRAP activity and the number of TRAP positive-multinuclear cells were quantified. The expression level of anti-oxidant gene (*SOD1* and *SOD2*) was assessed by RT-PCR. (d) The expression levels of osteoclast differentiation markers and transcription factor (*TRAP, DC-STAMP*, and *NFATc1*), and cartilage degradation enzymes (*MMP9, Adamts4*, and *Adamts5*) in OA chondrocytes co-cultured with osteoclasts in presence of Con or M-PD hydrogels were assessed by RT-PCR. (e) The protein level of NFATc1 and MMP9 were determined using Western blot assays and MMP-9 secretion was determined by zymography (right panel). β-Actin was the internal control. A schematic diagram summarizes the role of the M-PD hydrogel in inhibiting osteoclast differentiation and cartilage degradation (left panel). Values are Mean ± SD, $^{*}p < 0.05$, $^{**}p < 0.01$, $^{***}p < 0.001$, and $^{****}p < 0.0001$ by Student's *t* test.

which showed diminished light intensity between the Burr Hole_M-PD hydrogel (1.44 mW) and the DMM/Burr Hole_M-PD hydrogel (0.89 mW). Unlike the M-PD hydrogel, the Con gel showed low conductivity with no change in light intensity observed (Burr Hole/Con gel: 0.57 mW, DMM/Burr Hole_Con gel: 0.51 mW; Figure 7(b)). Confocal microscopy further verified that the quenched fluorescence in the M-PD hydrogel was revived owing to the high ROS concentration in the OA model mice of the Burr Hole and DMM/Burr Hole groups, demonstrating the sensitivity of the M-PD hydrogel in detecting OA. Immunohistochemical analysis of the skin tissue following subcutaneous transplantation of the M-PD gel assessed biocompatibility by measuring the expression of F4/80 (a macrophage marker), caspase-3 (an apoptosis marker), and Ki67 (a proliferation marker), which suggested favorable biocompatibility (Supplementary Figure 6).

To explore the role of osteoclasts in osteoarthritis development, we punctured a burr hole in the proximal tibia of a mouse and applied an M-PD hydrogel (Figure 8(a)). The induced bone defect led to an increase in the formation of osteoclasts within the trabecular bone (Figure 8(b)) and escalated cartilage matrix degradation (Figure 8(c)). However, the application of the M-PD hydrogel significantly reduced both osteoclast differentiation and formation, as well as cartilage matrix breakdown. This treatment did not influence growth plate zone length or cell number (Figure 8(d)). The relationship between osteoarthritic chondrocytes and osteoclasts was further explored (Figure 9(a)). DMM surgery was performed to induce osteoarthritis in animal models of burr hole-mediated bone defect, leading to an augmented breakdown of the cartilage matrix and a significant increase in osteoclast formation (Figure 9(b) and (c)). Remarkably, the M-PD hydrogel application drastically decreased both cartilage matrix degradation and osteoclast formation. Consistent with previous findings in Figure 8(d), the application of the M-PD hydrogel did not alter the growth plate zone length or cell numbers

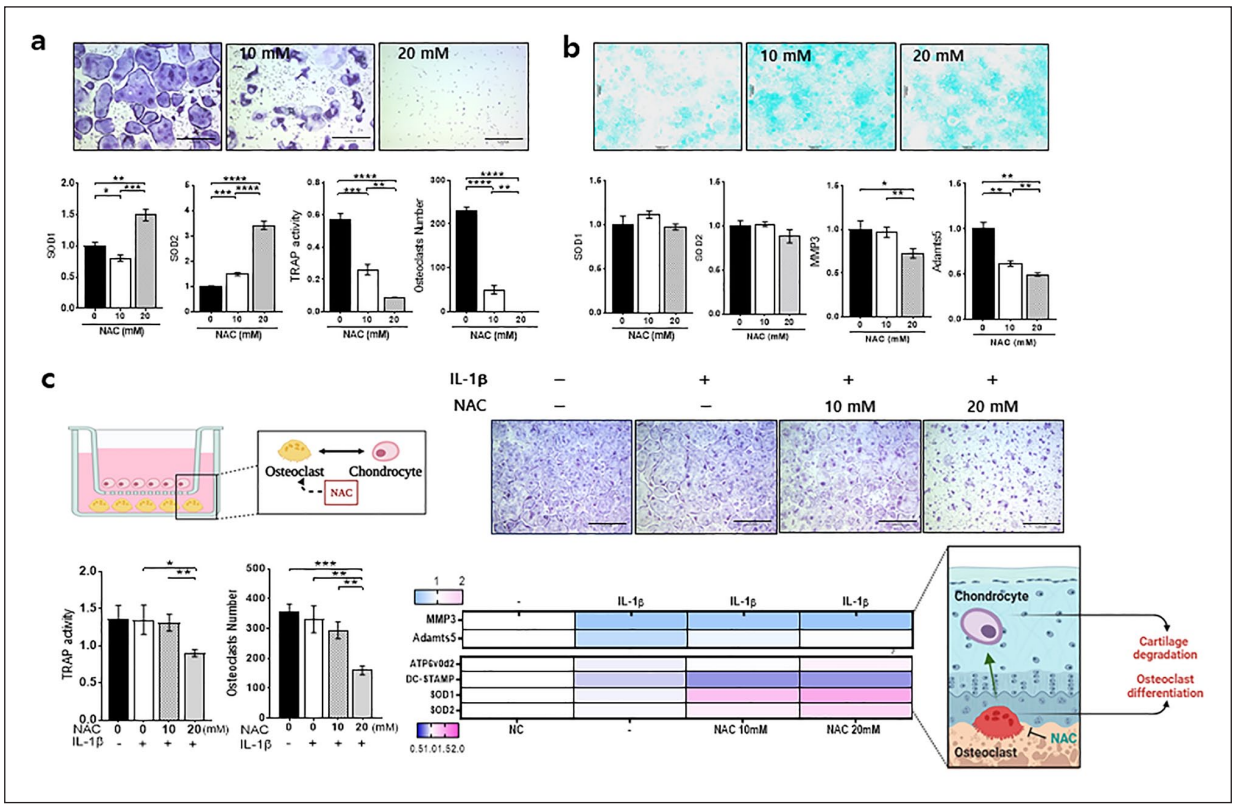

Figure 6. Impacts of NAC on osteoclast and osteoarthritic chondrocyte interaction. (a) Representative TRAP staining images of Osteoclasts with or without *N*-acetyl-L-cysteine (NAC) at varying concentrations (0, 10, and 20 mM). $n = 3$ per group. The expression level of anti-oxidant gene (*SOD1* and *SOD2*) was assessed by RT-PCR. TRAP activity and the number of TRAP positive-multinuclear cells were quantified. (b) Representative Alcian Blue staining images of chondrocytes with or without *N*-acetyl-L-cysteine (NAC) at varying concentrations (0, 10 mM, 20 mM). $n = 3$ per group. The expression level of anti-oxidant gene (*SOD1* and *SOD2*) and cartilage matrix-degrading enzyme genes (*MMP3* and *ADAMTS5*) in NAC treated iMAC cells was assessed by RT-PCR. (c) The schematic illustration of the experimental setup for the co-culture of osteoclasts and IL-1β-treated chondrocytes with NAC treatment and representative TRAP staining images of Osteoclasts (upper panel). TRAP activity and the number of TRAP positive-multinuclear osteoclasts were quantified. The expression levels of osteoclasts differentiation marker (*ATP6V0d2* and *DC-STAMP*) and oxidative stress-related genes (*SOD1* and *SOD2*) in osteoclasts and the expression of cartilage matrix-degrading enzymes genes (*MMP3* and *ADAMTS5*) in OA chondrocytes were assessed by real-time PCR and represented as a heatmap. Red denotes higher expression and blue denotes lower expression. A diagram outlines the proposed mechanism of NAC's action in reducing ROS levels, thereby affecting osteoclast differentiation and protecting against cartilage degradation. Values are Mean ± SD, $*p < 0.05$, $**p < 0.01$, $***p < 0.001$, and $****p < 0.0001$, N.S, not significant by Student's *t* test.

(Figure 9(d)). These findings suggest that targeting ROS scavenging by osteoclasts can modify the pathological progression of joint degeneration, offering the dual therapeutic advantage of maintaining cartilage integrity and regulating osteoclast differentiation and formation. This innovative strategy could redefine the management approaches for conditions such as osteoarthritis, in which current therapies primarily focus on symptom relief without addressing the cause of disease progression.

Discussion

Osteoarthritis is characterized by cartilage deterioration accompanied by changes in the subchondral bone and inflammation of synovial tissues.[24] Osteoclasts, responsible for bone and cartilage resorption, and chondrocytes, central to cartilage synthesis and maintenance, play critical roles in the pathogenesis of OA.[25] An imbalance in the activity of these cells typically contributes to disease development. Our approach focused on the modulation of ROS, a key factor in both osteoclastic bone resorption and cartilage degradation pathways. Elevated ROS levels are commonly observed in patients with OA and exacerbate inflammatory and catabolic processes.[26]

In this study, we explored the effectiveness of controlling ROS by implementing a manganese dioxide polymer dot (MnO2-PD) to modulate osteoclast differentiation and its potential implications in osteoarthritis (OA) progression. Our results demonstrate the ability of the hydrogel to inhibit osteoclast differentiation, as indicated by decreased the expression of NFATc1, a master transcription factor for osteoclastogenesis and downregulation of key osteoclast

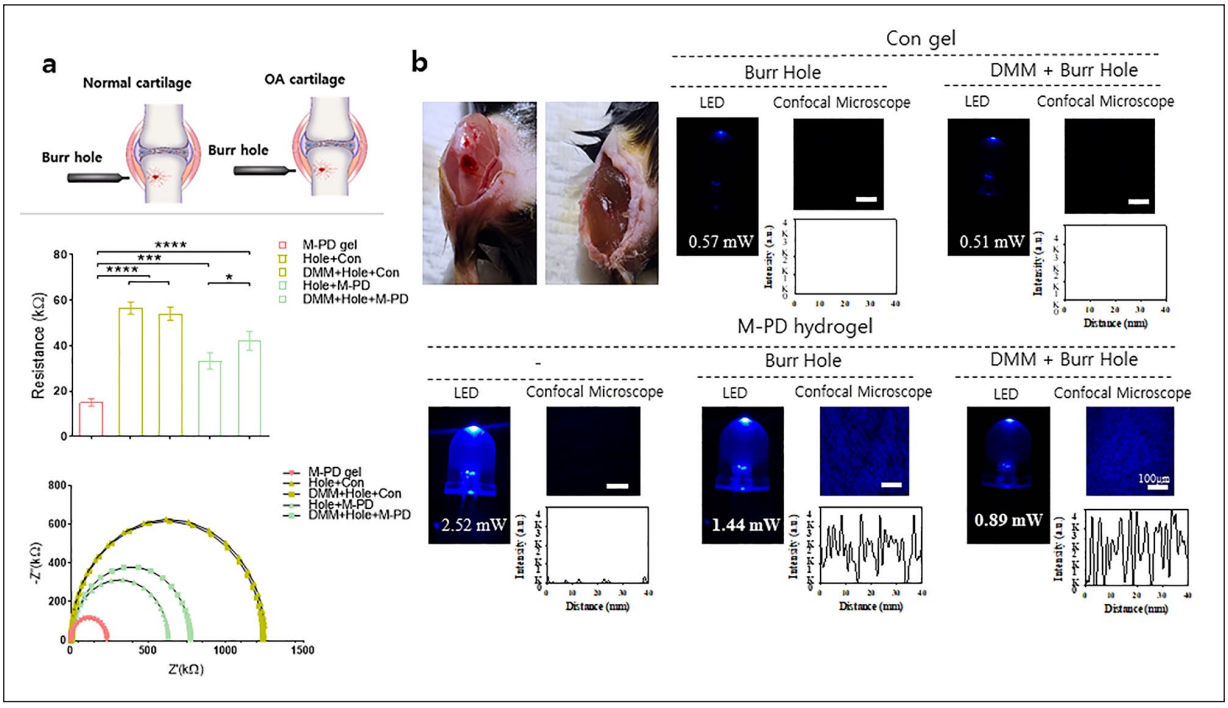

Figure 7. In vivo electrochemical sensing of osteoarthritis and bone defect using M-PD hydrogel. (a) The illustration and photographs of the procedure in normal cartilage vs. OA (DMM) cartilage. Electrical resistance measurement by sourcemeter and electrochemical impedance spectroscopy (EIS) obtained from Control and M-PD hydrogels implanted in mouse models (Burr Hole and DMM/Burr Hole, $n = 3$. (b) In vivo imaging and LED intensity and confocal microscopy analysis. Values are Mean ± SD, $^{*}p < 0.05$, $^{**}p < 0.01$, $^{***}p < 0.001$, and $^{****}p < 0.0001$ by Student's t test.

markers such as TRAP, OSCAR, CTSK, DC-STAMP, and ATP6V0D2. This is significant because osteoclasts are crucial for bone and cartilage resorption and are directly linked to the pathophysiology of OA, suggesting that the M-PD hydrogel could play a therapeutic role in maintaining the integrity of articular cartilage. The interplay between osteoclasts and chondrocytes in OA is complex and multifaceted. Co-culture experiments offer valuable insights into the impact of hydrogels on this interaction. Remarkably, the presence of the M-PD hydrogel not only inhibited osteoclast differentiation but also seemed to shield chondrocytes by reducing the expression of matrix-degrading enzymes.

This dual protective mechanism suggests that ROS modulation could effectively slow the progression of OA, shifting the balance toward joint preservation rather than degradation. By maintaining a more balanced oxidative stress environment, the hydrogel helps sustain joint integrity and function. This outcome indicates the potential for broader therapeutic applications, suggesting that similar ROS-targeting strategies can be tailored to other inflammatory and degenerative conditions. Furthermore, our approach aligns with current trends in OA treatment, which advocate for multi-target strategies rather than single-target interventions.

Given the multifactorial nature of OA, which involves mechanical, genetic, and biochemical factors, our strategy underscores the need to address multiple pathways simultaneously. The interplay between mechanical stress and biochemical processes, particularly the role of oxidative stress in perpetuating the inflammatory response, provides a comprehensive framework for our discussion. This integration of therapeutic targets, therefore, not only halts disease progression but also initiates recovery processes, fostering a regenerative environment in joint tissues. Our insights into the role of ROS in osteoclast differentiation and their interactions with chondrocytes offer a promising therapeutic avenue for OA treatment. This potential dual action in OA pathogenesis may contribute to the development of novel and effective treatment strategies. Our findings underscore the importance of understanding the cellular and molecular mechanisms underlying the pathogenesis of OA. The impact of hydrogels in reducing oxidative stress within osteoclasts and altering their interaction with chondrocytes opens new avenues for targeted therapeutic strategies in OA.

Our study builds on a robust foundation of research exploring the roles of ROS in OA and the therapeutic potential of various biomaterials in modulating disease progression. Previous studies have demonstrated that elevated ROS levels contribute significantly to the pathogenesis of OA by promoting oxidative stress, inflammation, and cartilage degradation.[27–29] Our findings align with this, emphasizing the critical role of ROS in osteoclast differentiation

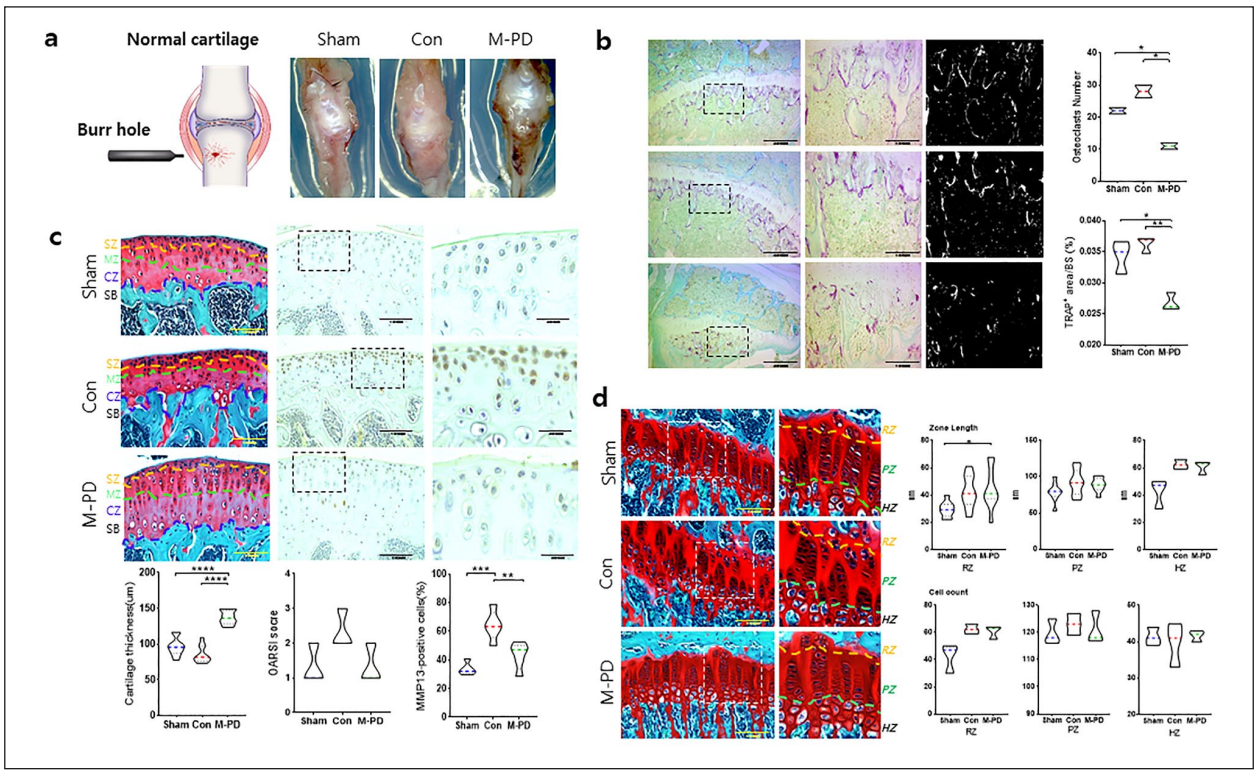

Figure 8. The Role of M-PD Hydrogel in modulating osteoclast formation and cartilage degradation post-burr hole injury in mouse tibia. (a) The illustration and photographs of the procedure of creating a burr hole in the proximal mouse tibia, followed by the application of M-PD hydrogel. (b) Representative TRAP staining images of the mouse tibia. The number and area on bone surface of TRAP(+)-multinuclear osteoclasts were quantified. (c) Representative images of Safranin O staining and immunohistochemistry of MMP-13. Cartilage thickness, OARSI scores, and percentage of MMP-13 positive cells were quantified. (d) Representative histological images growth plates. The length and cell number in different zones (RZ, PZ, and HZ) were quantified. $n = 4$ per group, Values are Mean ± SD, *$p < 0.05$, **$p < 0.01$, ***$p < 0.001$, and ****$p < 0.0001$, N.S, not significant by Student's t test.

and chondrocyte protection. The incorporation of manganese dioxide-polymer dot (MnO2-PD) nanoparticles in hydrogels as ROS scavengers has been demonstrating the dual therapeutic effects on both osteoclasts and chondrocytes, thus offering a comprehensive strategy for managing OA. While our study presents promising results, several limitations need to be addressed. Further in vivo studies and clinical trials are needed to confirm the efficacy and safety of the M-PD hydrogel in human subjects. In addition, the long-term stability and biodegradability of the M-PD hydrogel remain uncertain. Chronic conditions like OA require long-term treatment, and any biomaterial used must maintain its efficacy and biocompatibility over extended periods. While our study highlights the role of ROS scavenging in modulating osteoclast and chondrocyte activity, a deeper mechanistic understanding of how the M-PD hydrogel interacts with cellular signaling pathways is needed. Our study suggests that the M-PD hydrogel not only scavenges reactive oxygen species (ROS) but also potentially influences key signaling pathways involved in osteoclast regulation and osteoarthritis (OA) progression. One of the key pathways affected by ROS is the NF-kB pathway, which plays a crucial role in inflammation and osteoclast differentiation. The M-PD hydrogel, through its ROS-scavenging properties, can potentially inhibit the activation of the NF-kB pathway, thereby reducing the expression of pro-inflammatory cytokines and osteoclast-related genes. Additionally, the MAPK pathway, which is another critical regulator of osteoclastogenesis and inflammation, can be influenced by changes in ROS levels. By decreasing ROS, the M-PD hydrogel may attenuate the MAPK signaling cascade, which includes ERK, JNK, and p38 MAPK, leading to suppressed osteoclast differentiation and activity. Our findings indicate that treatment with the M-PD hydrogel leads to downregulation of key osteoclast differentiation markers and transcription factors, such as NFATc1, which are downstream targets of both NF-κB and MAPK signaling. This suggests that the hydrogel may exert its effects by modulating these pathways, thereby altering the osteoclastogenic microenvironment in OA. By integrating the modulation of ROS with the regulation of these critical signaling pathways, the M-PD hydrogel holds promise as a comprehensive therapeutic approach for controlling osteoclast activity and managing OA progression. Further research is needed to elucidate the precise molecular mechanisms and confirm the hydrogel's effects on these

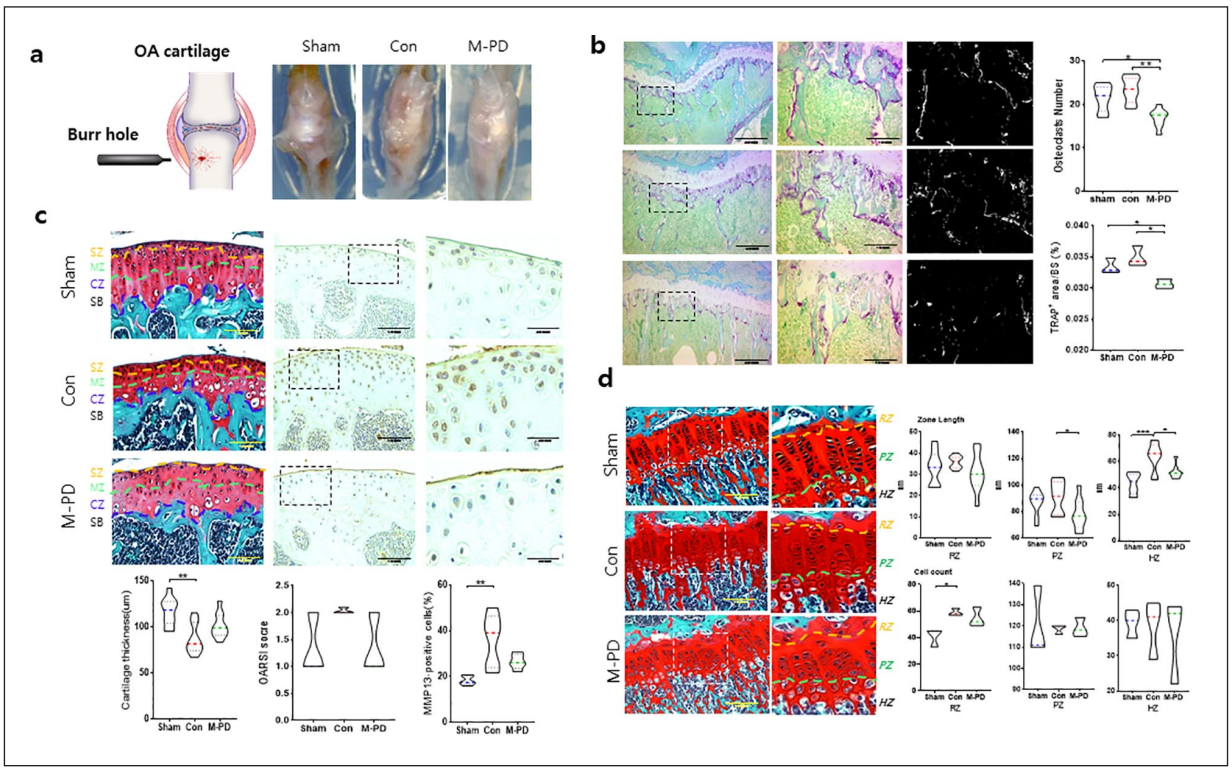

Figure 9. Impact of M-PD hydrogel on cartilage degradation and osteoclast formation post-burr hole bone defect under OA condition. (a) The illustration and photographs of the procedure for inducing osteoarthritis through DMM surgery and bone defect by Burr holes simultaneously, followed by the application of the M-PD hydrogel. (b) Representative TRAP staining images of the mouse tibia. The number and area on bone surface of TRAP(+)-multinuclear osteoclasts were quantified. (c) Representative images of Safranin O staining and immunohistochemistry of MMP-13. Cartilage thickness, OARSI scores, and percentage of MMP-13 positive cells were quantified. (d) Representative histological images growth plates. The length and cell number in different zones (RZ, PZ, and HZ) were quantified. $n = 4$ per group, Values are Mean ± SD, $^{*}p < 0.05$, $^{**}p < 0.01$, $^{***}p < 0.001$, and $^{****}p < 0.0001$, N.S, not significant by Student's *t* test.

pathways in vivo, but these initial findings provide a strong foundation for its potential therapeutic application.

Conclusion

This study demonstrated that the M-PD hydrogel effectively scavenges ROS, thus modulating the joint microenvironment to inhibit osteoclast differentiation and protect cartilage integrity in OA. The dual functionality of the hydrogel was highlighted by its ability to decrease osteoclast formation and cartilage matrix degradation in both in vitro and in vivo models. By mitigating ROS levels, the hydrogel not only prevented the differentiation and formation of osteoclasts but also preserved the structural and functional properties of chondrocytes. These findings suggest that targeting ROS with hydrogels can serve as a promising therapeutic strategy for OA, providing the dual benefit of protecting the structural integrity of the joint while controlling the biochemical pathways that exacerbate the disease process. The potential of the M-PD hydrogel in OA treatment could transform current therapeutic approaches from mere symptom relief to modifying disease progression at the molecular level.

Author contributions

S. J., T.K., and G.K. contributed equally to this work. S. J. and J. P.: formal analysis, methodology, and data curation for chondrocytes. G.K.: formal analysis, methodology, and data curation for osteoclasts. T.K.: formal analysis, methodology, and data curation for M-PD hydrogel. S.P., S.L., and E-J. J.: conceptualization, data curation, supervision, and writing draft.

Data availability

The datasets generated and/or analyzed in the current study are available from the corresponding author upon reasonable request.

Declaration of conflicting interests

The author(s) declared no potential conflicts of interest with respect to the research, authorship, and/or publication of this article.

Funding

The author(s) disclosed receipt of the following financial support for the research, authorship, and/or publication of this article: This work was supported by National Research Foundation of Korea (NRF) grants funded by the Korean Government (MSIT) Nos. 2022R1A4A1031259 and 2021R1I1A3041149 to E-J. J. and No. RS-2023-00207925 and 2018R1A6A1A03023788 to S. P.

ORCID iD

Eun-Jung Jin https://orcid.org/0000-0002-6874-3017

Supplemental material

Supplemental material for this article is available online.

References

1. Jiang Y. Osteoarthritis year in review 2021: biology. *Osteoarthritis Cartilage* 2022: 30: 207–215.
2. Gong Y, Qiu J, Ye J, et al. AZ-628 delays osteoarthritis progression via inhibiting the TNF-α-induced chondrocyte necroptosis and regulating osteoclast formation. *Int Immunopharmacol* 2022; 111: 109085.
3. Agidigbi TS and Kim C. Molecular sciences reactive oxygen species in osteoclast differentiation and possible pharmaceutical targets of ROS-mediated osteoclast diseases. *Int J Mol Sci* 2019; 20(14): 3576.
4. Fu Y, Cui S, Zhou Y, et al. Dental pulp stem cell-derived exosomes alleviate mice knee osteoarthritis by inhibiting TRPV4-mediated osteoclast activation. *Int J Mol Sci* 2023; 24: 4926.
5. Arra M, Swarnkar G, Ke K, et al. LDHA-mediated ROS generation in chondrocytes is a potential therapeutic target for osteoarthritis. *Nat Commun* 2020; 9: 3427.
6. Zarkovic N. Roles and functions of ROS and RNS in cellular physiology and pathology. *Cells* 2020; 9: 767.
7. Yunus Ansari M, Ahmad N and Haqqi TM. Oxidative stress and inflammation in osteoarthritis pathogenesis: role of polyphenols. *Biomed Pharmacother* 2020; 129: 110452.
8. Chen H, Tan XN, Hu S, et al. Molecular mechanisms of chondrocyte proliferation and differentiation. *Front Cell Dev Biol* 2021; 9: 664168.
9. Jin Z, Chang B, Wei Y, et al. Curcumin exerts chondroprotective effects against osteoarthritis by promoting AMPK/PINK1/Parkin-mediated mitophagy. *Biomed Pharmacother* 2022; 151: 113092.
10. Wang S, Deng Z, Ma Y, et al. The role of autophagy and mitophagy in bone metabolic disorders. *Int J Biol Sci* 2020; 16: 2675–2691.
11. Kim JM, Lin C, Stavre Z, et al. Osteoblast-osteoclast communication and bone homeostasis. *Cells* 2020; 9: 2073.
12. Zhao K, Ruan J, Nie L, et al. Effects of synovial macrophages in osteoarthritis. *Front Immunol* 2023; 14: 1164137.
13. Shangguan L, Ding M, Wang Y, et al. Denosumab ameliorates osteoarthritis by protecting cartilage against degradation and modulating subchondral bone remodeling. *Regen Ther* 2024; 27: 181–190.
14. Rajesh I, Sandhya Bhavani P and Abhinav A. Novel therapies for osteoarthritis treatment: an overview of recent developments. *Ortho Rheum Open Access J* 2023; 22(2): 556081.
15. Poljsak B, Šuput D and Milisav I. Achieving the balance between ROS and antioxidants: when to use the synthetic antioxidants. *Oxid Med Cell Longev* 2013; 2013: 956792.
16. Guo X, Xi L, Yu M, et al. Regeneration of articular cartilage defects: therapeutic strategies and perspectives. *J Tissue Eng* 2023; 14: 20417314231164765.
17. Shajib MS, Futrega K, Jacob Klein T, et al. Collagenase treatment appears to improve cartilage tissue integration but damage to collagen networks is likely permanent. *J Tissue Eng* 2022; 13: 20417314221074207.
18. Cho WJ, Ahn J, Lee M, et al. Combinatorial effect of mesenchymal stem cells and extracellular vesicles in a hydrogel on cartilage regeneration. *Tissue Eng Regen Med* 2023; 20(1): 143–154.
19. Dou H, Wang S, Hu J, et al. Osteoarthritis models: from animals to tissue engineering. *J Tissue Eng* 2023; 14: 20417314231172584.
20. Gi Kim S, Song J, Ryplida B, et al. Touchable electrochemical hydrogel sensor for detection of reactive oxygen species-induced cellular senescence in articular chondrocytes. *Adv Funct Mater* 2023; 33: 2213887.
21. Li Z and Helms JA. Drill hole models to investigate bone repair. *Methods Mol Biol* 2021: 2221: 193–204.
22. Kim SG, Song J, Ryplida B, et al. Touchable electrochemical hydrogel sensor for detection of reactive oxygen species-induced cellular senescence in articular chondrocytes. *Adv Funct Mater* 2023; 33: 2213887.
23. Zhou Y, Zhang Y, Wang H, et al. Microglial pyroptosis in hippocampus mediates sevolfurane-induced cognitive impairment in aged mice via ROS-NLRP3 inflammasome pathway. *Int Immunopharmacol* 2023; 116: 109725.
24. Li G, Yin J, Gao J, et al. Subchondral bone in osteoarthritis: insight into risk factors and microstructural changes. *Arthritis Res Ther* 2013; 15: 223.
25. Park DR, Kim J, Kim GM, et al. Osteoclast-associated receptor blockade prevents articular cartilage destruction via chondrocyte apoptosis regulation. *Nat Commun* 2020; 11: 4343.
26. Lepetsos P and Papavassiliou AG. ROS/oxidative stress signaling in osteoarthritis. *Biochim Biophy Acta* 2016; 1862: 576–591.
27. Henrotin Y, Clutterbuck AL, Allaway D, et al. Biological actions of curcumin on articular chondrocytes. *Osteoarthritis Cartilage* 2010; 18(2): 141–149.
28. Hunter DJ and Bierma-Zeinstra S. Osteoarthritis. *Lancet* 2019; 393(10182): 1745–1759.
29. Kapoor M, Martel-Pelletier J, Lajeunesse D, et al. Role of proinflammatory cytokines in the pathophysiology of osteoarthritis. *Nat Rev Rheumatol* 2011; 7(1): 33–42.